

Cite this article as: Chang Limei, Zhang Shizhou, Wen Qian, et al. Effects of Corrosion Product MgO on Corrosion Resistance of Fe-based Alloys in Solid and Molten NaCl-MgCl₂ at High Temperature[J]. Rare Metal Materials and Engineering, 2022, 51(12): 4452-4463.

ARTICLE

Effects of Corrosion Product MgO on Corrosion Resistance of Fe-based Alloys in Solid and Molten NaCl-MgCl₂ at High Temperature

Chang Limei¹, Zhang Shizhou¹, Wen Qian¹, Xi Jihui¹, Wu Bo², Wang Junwei^{2,3}

¹Department of Mechanical Engineering, Qinghai University, Xining 810016, China; ²Xiamen Key Laboratory of Marine Corrosion and Smart Protective Materials, Jimei University, Xiamen 361021, China; ³Engineering Research Center of High Performance Light Metal Alloys and Forming, Qinghai University, Xining 810016, China

Abstract: Molten chloride salt is a candidate heat transfer medium (HTM) for the next generation high temperature concentrating solar power (CSP). A corrosion product MgO will be formed on metal surface in the molten chloride containing MgCl₂. Based on the corrosion behavior comparison of a carbon steel and three kinds of Fe-Cr-Ni alloys in solid (345 °C) and molten state NaCl-MgCl₂ (445 and 545 °C), the effects of MgO on corrosion resistance of the four kinds of samples were discussed. Results show that in solid eutectic NaCl-MgCl₂ at 345 °C, the MgO layer is dense and complete on the carbon steel surface, which can protect the specimen from corrosion. In the molten salt, a dense MgO layer is also formed on the four kinds of sample surface, but the molten salt penetrates the MgO/matrix interface along cracks of the oxide layer due to the peeling off of MgO layer under thermal stress, which cannot protect specimen from corrosion. The corrosion mechanism is the chemical-electrochemistry reactions.

Key words: Fe-Cr-Ni alloy; carbon steel; molten chloride; corrosion; MgO

The solar energy heat transfer medium (HTM) and storage medium by phase change material (PCM) are based on molten chloride salts, because of their high thermal stability, low cost and proper melting point^[1-3]. Molten chloride is also a candidate HTM for the third generation CSP based on the supercritical carbon dioxide (sCO₂) Brayton cycle because of high CSP system thermo-electric conversion efficiency^[4]. But the metal pipe and container will be corroded severely by the chloride salt under impurity water vapor and oxygen, which restricts the technology development of the molten salt phase change thermal energy storage^[5-8].

In actual operation, because of high cost and technical difficulty, it is difficult to remove the impurity water vapor and oxygen in tons of molten chloride salt HTM or PCM thoroughly^[9-13]. The water vapor and oxygen in air atmosphere have serious effects on metal corrosion process^[14,15]. The eutectic NaCl-52wt% MgCl₂ ($T_m=445$ °C) has wide

development prospect because of low cost, good physical and chemical stability, relatively high melting latent heat per unit mass (430 J/g), etc^[6,16]. In our previous experiments, after metal is corroded in the molten salt, MgO crust or particles form obviously on the sample surface in the molten salt^[5,11]. Except for the molten NaCl-MgCl₂, in other types of HTM or PCM molten chloride salts containing MgCl₂ (NaCl-KCl-MgCl₂, KCl-MgCl₂, NaCl-CaCl₂-MgCl₂, etc), although the molten salt is protected under an argon atmosphere and/or the corrosion container is sealed by weld, the MgO particle or crust also forms on the container inner surface after corrosion experiment^[17-20].

The corrosion behavior of Fe-based and Ni-based alloys in molten KCl-32at% MgCl₂, NaCl-CaCl₂-MgCl₂ under air atmosphere has been studied. They are corroded severely for the chromium chloride outward diffusion^[20,21]. After a pre-oxidation treatment, a double oxide layer (Cr₂O₃ and Al₂O₃) is

Received date: January 10, 2022

Foundation item: National Natural Science Foundation of China (51441003); Qinghai Natural Science Foundation (2015-ZJ-931Q); Research Foundation of Jimei University (ZQ2021052); National Key Research and Development Program (2020YFE0100100)

Corresponding author: Wang Junwei, Ph. D., Professor, Xiamen Key Laboratory of Marine Corrosion and Smart Protective Materials, Jimei University, Xiamen 361021, P. R. China, Tel: 0086-592-6183532, E-mail: 202161000046@jmu.edu.cn

Copyright © 2022, Northwest Institute for Nonferrous Metal Research. Published by Science Press. All rights reserved.

formed on In702, HR224 and APMT surface, which improves corrosion resistance in molten MgCl_2 -64.41wt% KCl at 700 °C at initial corrosion stage. But the sample matrix under the Al_2O_3 layer is porous. The oxide layer easily peels off after corrosion for hundreds of hours^[19,22]. Compared with pure Al and Cu, the corrosion resistance of the stainless steel (316L) is the best in molten hydrates bischofite ($\text{MgCl}_2 \cdot 6\text{H}_2\text{O}$) salt^[23]. Alloy elements Cr and C play an important role in the corrosion process of stainless steel in molten chloride^[24,25]. The corrosion behavior of Fe-, Ni- and Co-based typical alloys in molten NaCl-MgCl₂ has been studied by our research team, and the influence of MgO on the corrosion behavior cannot be ignored^[26-28]. Ni-Mo-Cr alloy is corroded more serious in gas NaCl-KCl-MgCl₂ salt than in the molten salt, for the oxidation of Mg chloride^[29,30].

As a HTM or PCM, it is going to work in the solid, liquid and gas state phases at high temperature. The corrosion behavior differences of Fe-based alloys in solid and molten NaCl-MgCl₂ are unclear. The effect of the corrosion product MgO crust on the corrosion resistance of Fe-based alloys in the solid and molten chloride is unclear too. Consequently, taking a carbon steel with high content of carbon (T8) and three kinds of low cost (relative to Ni-based alloy) Fe-Cr-Ni alloys (simulating the main composition of stainless steel ASTM 201, 304 and 321) as specimens, their corrosion behavior in the solid (at 345 °C) and molten (at 445 and 545 °C) eutectic salt (NaCl- MgCl₂) was compared. The MgO crust formation process and its effect on those sample surface at different temperatures were discussed.

1 Experiment

Carbon steel (T8) samples were cut from a steel board, which was bought from market. Referencing to the content of main alloy elements Fe, Cr and Ni of stainless steels 201, 304 and 321 in ASTM A959-2004, the compositions of three kinds of analog Fe-Cr-Ni alloys used in the experiment are listed in Table 1. They are labeled as 201, 304 and 321. Taking pure Fe, Ni and Cr (purity>99.9%) as raw materials, three kinds of alloy ingots were made by the medium frequency induction melting furnace (type: SP-25TC). All specimens were cut into small pieces with the dimension of 10 mm×10 mm×3 mm by wire electric discharge machining. The samples' actual composition was detected by X-ray fluorescence (XRF, ZSX Primus II*), which

is listed in Table 1 too. In order to show the microstructure (metallography) of the four kinds of initial specimens, the as-received carbon steel and three kinds of Fe-Cr-Ni specimens were corroded by the nital ($\text{CH}_3\text{CH}_2\text{OH}+5\text{vol}\% \text{HNO}_3$) and the aqua regia ($\text{HCl}:\text{HNO}_3=3:1$, volume fraction), respectively.

There were five parallel specimens for every kind of alloys. Their surface areas and mass were measured by a vernier caliper (Hengliang-530-150, accuracy 0.02 mm, Shanghai Hengliang Measuring Tool Co., Ltd) and an electronic balance (SOPTOP-FA2004, accuracy 0.01 mg, Shanghai Sunny Hengping Scientific Instrument Co., Ltd), respectively. Analytically pure MgCl_2 and dried analytically pure NaCl were mixed in proportion of NaCl-52wt% MgCl_2 . The mixed salt was put in four alumina crucibles. Then the four crucibles were put into a muffle furnace which had been heated to 545 °C. After the mixed salt melted totally, the four kinds of specimens were submerged in the molten salt totally in the four crucibles. For the corrosion experiments at 345 °C, the four crucibles with specimens were put in a muffle furnace which had been heated to 345 °C. Similarly, for the corrosion experiments at 445 or 545 °C, the four crucibles with specimens were put in another muffle furnace which had been heated to 445 or 545 °C. Based on our previous corrosion experience, the metal in molten chloride will be corroded severely in a short exposure time^[26-28]. Consequently, only after exposure to corrosion for 10 h, these crucibles were taken out and cooled down to the room temperature. In addition, to generate corrosion product MgO more obviously, air atmosphere was chosen during the corrosion process. The corrosion residual salt was collected and then detected by X-ray diffractometer (XRD, Rigaku D/max-2500/PC X-ray, Cu K α radiation source, $\lambda=0.1541 \text{ nm}$). The metal specimens with a residual salt were cleared by the submerged-water method^[11,27]. Repeat above process for 8 times. After the first corrosion exposure experiment, one specimen was firstly detected by XRD (Rigaku D/max-2500/PC), and then its morphology was observed by a scanning electron microscope (SEM, ZEISS MERLIN Compact and JSM-6610 LV) equipped with energy dispersive spectrometer (EDS). After the last corrosion exposure experiment, the cross section of one specimen which was not prepared by submerged-water method was analyzed by SEM equipped with EDS. More details of the experiment method and facilities are shown in Ref.[20].

Table 1 Nominal and tested compositions of samples by XRF

Sample	Cr			Ni			Ti			C	Fe
	Nominal /wt%	Tested		Nominal /wt%	Tested		Nominal /wt%	Tested			
		wt%	at%		wt%	at%		wt%	wt%		
T8	-	-	-	-	-	-	-	-	-	0.80	Bal.
201	14.5	14.7	15.7	4.5	4.3	4.1	-	-	-	-	Bal.
304	18.0	18.0	19.2	9.5	9.6	9.1	-	-	-	-	Bal.
321	18.0	19.6	20.8	4.5	5.4	5.1	1.0	0.8	0.9	-	Bal.

2 Results and Discussion

2.1 Experiments results

The relationships between the average mass change and the exposure time at 345 and 545 °C are shown in Fig. 1a and 1b, respectively. At 345 °C, the mass of T8 increases rapidly after exposure for 10 h, and then decreases slightly with the extension of the exposure time. But for the 201, 304 and 321 specimens, their mass decreases continuously. At 545 °C, the four kinds of specimen lose mass during the exposure process, and the specimen T8 is the most serious.

After corrosion for 10 h in the mixed salt at 345, 445 and 545 °C, the surface topography and EDS results at local position of specimen T8 are shown in Fig. 2a~2g. XRD results are shown in Fig. 2h. It is found from Fig. 2a that the specimen surface is covered by small globules MgO crust. After corrosion at 445 °C, as shown in Fig. 2b, a smooth and dense MgO crust is formed on the specimen surface too. After the oxide layer peels off locally, the sample matrix is exposed (region 2 in Fig. 2b). After corrosion in the molten salt at 545 °C, only small part of surface was covered by MgO crust. Under the MgO crust, a lot of Fe and a little O are also detected by EDS (region 2 in Fig. 2c). Corrosion grooves along the grain boundary are found in the magnified sample matrix (after the MgO crust peels off), as shown in Fig. 2d. The intergranular corrosion is also proved by cross sectional SEM images later.

The surface topography and EDS results of the specimen 201 after corrosion for 10 h in the mixed salt at 345, 445 and 545 °C are shown in Fig. 3a~3g. Fig. 3h is XRD results of

specimens. After exposure at 345 °C, a multilayer crust is formed on the specimen surface (Fig. 3a), the main composition is MgO on the outermost layer, and oxides of Mg, Cr and Fe (MgO , $\text{CrO}_{0.87}$) on the interlayer and matrix. After corrosion at 445 °C, it is found from Fig. 3b and XRD results in Fig. 3h that a MgO crust (position 2) with coarse surface is formed on the outermost layer of the specimen surface. But the coarse layer cracks and peels off seriously. Under the MgO crust, a dense and smooth MgO interlayer (position 1) is exposed. A little Cr (12.1at%) is also found on the interlayer, and the interlayer cracks too. As marked by hollow arrows in Fig. 3b, a fracture is found on the MgO arch. After the interlayer peels off partly, the specimen matrix is exposed, where the content of Ni (5.1at%) is higher than that in the original specimen (4.1at%), but the content of Cr (11.2at%) is lower than that in the original specimen (15.7at%).

After corrosion at 545 °C, MgO crust is also formed on surface and peels off seriously, as shown in Fig. 3c. A little Cr is found on the MgO crust. But the content of Cr (4.3at%) on the MgO crust (position 1 in Fig. 3c) is lower than that on the inter layer (12.1at%) of specimen corroded at 445 °C. Under the crust, a porous matrix is exposed as shown in Fig. 3d. On the corroded matrix, compared with the composition of as-prepared specimen (Ni 4.3at%, Cr 15.4at%), the content of Ni (59.2at%) increases and Cr (3.8at%) decreases (position 2 in Fig. 3c). Many corrosion pits are found in the specimen matrix.

The surface topography and EDS results of the specimen 304 after corrosion at 345, 445 and 545 °C for 10 h are shown in Fig. 4a~4g. The XRD results of sample surface are shown in Fig. 4h. It is found that the three kinds of sample surface are covered by MgO crust. After corrosion at 345 °C, cracked bag swellings which are rich in Cl (5.4at%) and Na (1.5at%) are found on the MgO crust (position 1 in Fig. 4a). After corrosion at 445 and 545 °C, the arched MgO crust peels off locally because of squeezing, which is marked by hollow arrows in Fig. 4b and 4c. It is found in Fig. 4d which is magnified topography of Fig. 4c that the corrosion along grain boundary and corrosion pits are also found in the sample matrix after the MgO crust is squeezed off.

The surface topography and EDS result of specimen 321 after corrosion at 345, 445 and 545 °C for 10 h are shown in Fig. 5a~5g. The XRD results of these specimens are shown in Fig. 5h. A MgO crust is formed on three kinds of sample surface. There are many MgO particles on the sample surface after corrosion at 350 °C (Fig. 5a). An arched MgO crust is also found in Fig. 5c, which is marked by hollow arrows. The magnified SEM surface topography of the specimen 321 after corrosion at 545 °C for 10 h is shown in Fig. 5d. The sample surface is porous. A scraggly specimen matrix is exposed after the crust peels off.

Overall, there are two same features for the three kinds of stainless steel (201, 304 and 321) specimens after corrosion at 445 and 545 °C. First, the contents of Cr in the smooth oxide crust on the three kinds of stainless steel surface after exposure at 445 °C (position 1 in Fig. 3b, Fig. 4b and Fig. 5b) are higher than that at 545 °C (position 1 in Fig. 3c, Fig. 4c and

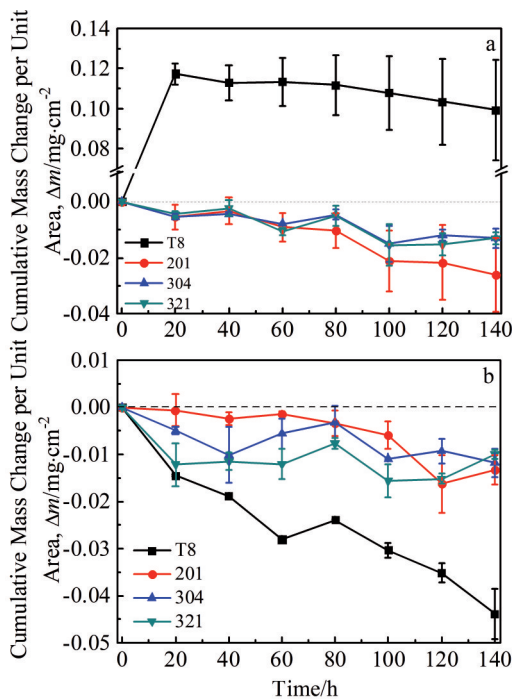


Fig.1 Relationship between the mass change and exposure time for four specimens at different temperatures: (a) 345 °C and (b) 545 °C

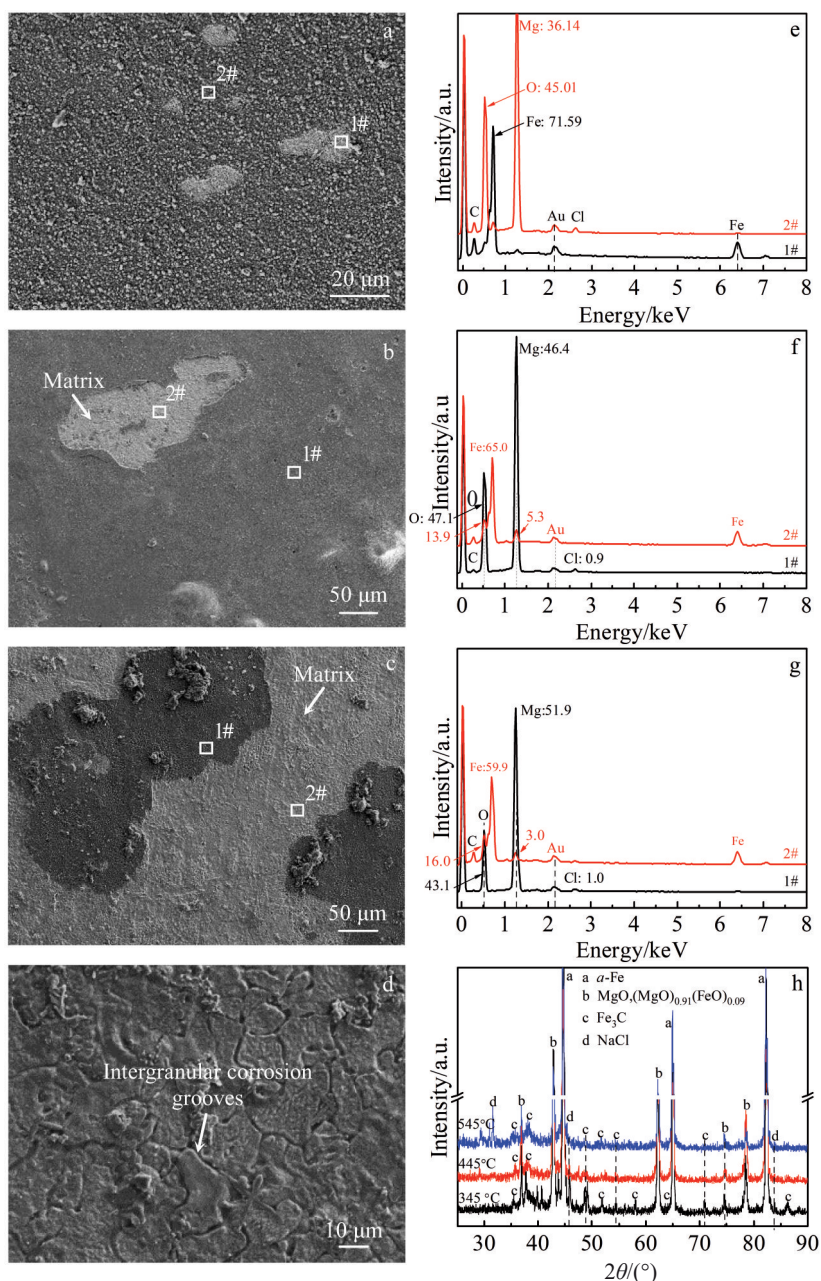


Fig.2 SEM images (a~d), EDS spectra (e~g) and XRD patterns (h) of T8 specimen surface after corrosion at different temperatures for 10 h: (a, e) 345 °C, (b, f) 445 °C, and (c, d, g) 545 °C (numbers in Fig.2e~2g indicate relative content of the element in at%)

Fig.5c). The tendency is shown in Fig.6.

Second, comparing as-received specimens with 201, 304 and 321 specimens exposed at 445 and 545 °C, the content of Cr decreases and that of Ni increases in the exposed matrix after the MgO crust peels off. The content and change of elements in the exposed 304 matrix are listed in Table 2.

Cross section SEM images and EDS results of the four kinds of Fe-based alloy after corrosion at 345 and 545 °C for 80 h are shown in Fig. 7a~7h. For T8 specimen, as shown in Fig.7a, after corrosion at 345 °C for 80 h, the specimen matrix near the surface becomes incomplete, and the surface is covered by a thick MgO crust. After corrosion at 545 °C, the intergranular corrosion occurs seriously in the specimen

matrix near surface. The corrosion pits are filled by the MgO.

It is found from Fig.7c that the 201 specimen matrix near surface is incomplete too. The specimen surface is also covered by MgO crust. The change of the element content of Fe, Cr and Ni is not evident. After corrosion at 545 °C for 80 h, as shown in Fig.7d, a gap about 15 μm between MgO layer and specimen matrix is formed. There is MgO crust at the region I, which is rich in Mg and O. At the region II, the content of Cr and Fe decreases from the matrix to surface, but the content Ni increases (region IV), where the microstructure is very loose. In addition, at the bottom of the region I (region IV), the content of Cr is slightly higher than the around.

As shown in Fig.7e, after the 304 specimen is corroded at

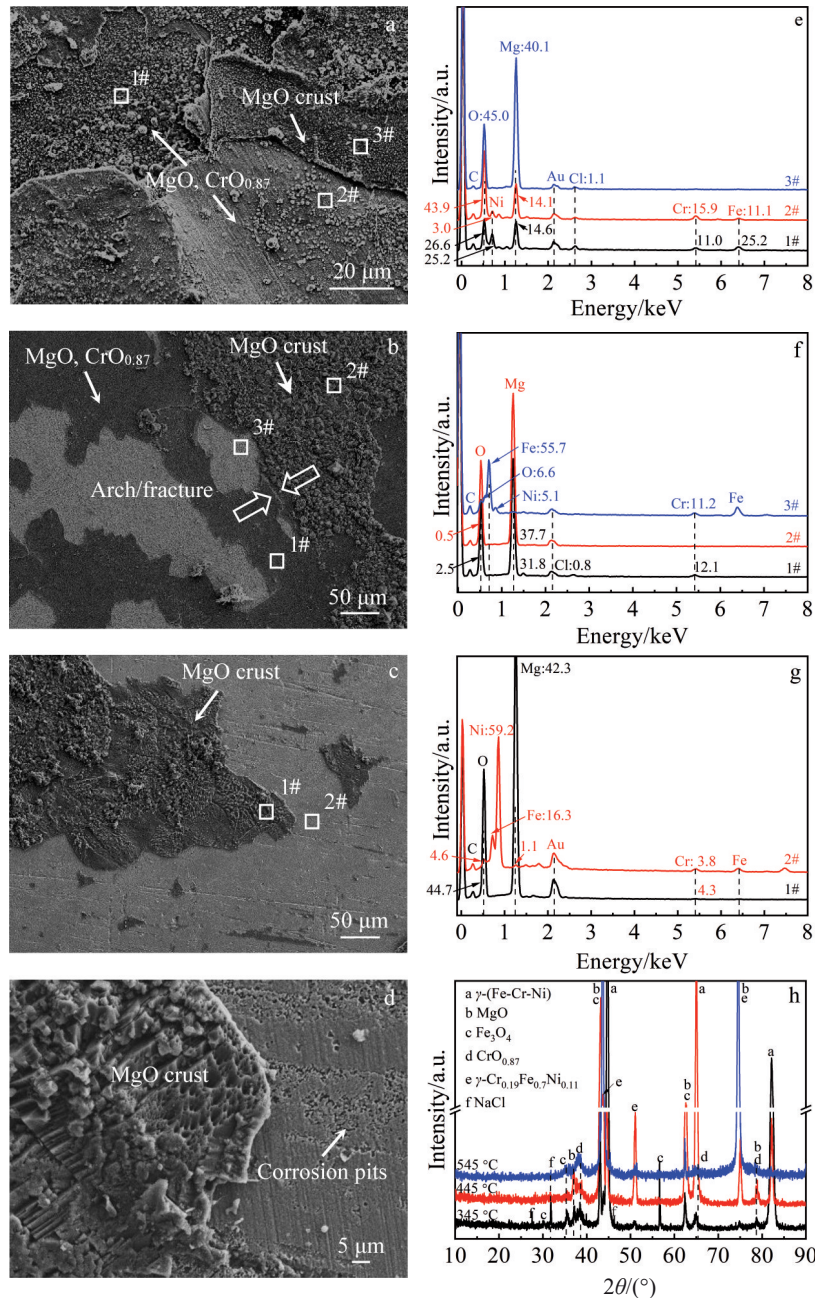


Fig.3 SEM images (a~d), EDS spectra (e~g) and XRD patterns (h) of 201 specimen surface after corrosion at different temperatures for 10 h: (a, e) 345 °C, (b, f) 445 °C, and (c, d, g) 545 °C (numbers in Fig.3e~3g indicate relative content of the element in at%)

345 °C, many small corrosion pits form on the specimen surface. After corrosion at 545 °C, as shown in Fig. 7f, the specimen surface is incomplete. At the region I, the content of Cr is lower and Ni is higher than those in the specimen matrix. There is a region II (about 8 μm) with high content of Cr on the specimen matrix near surface.

For the 321 specimen, after corrosion at 345 °C, the MgO crust also forms on the sample surface, and there is an obvious corrosion gap between the MgO crust and specimen matrix. After corrosion at 545 °C, as shown in Fig.7h, there is a MgO crust on the specimen surface, and the content of Cr also decreases on the sample matrix near the surface (region I). However, the content of Cr increases at region II (~8 μm).

The residual salt compositions (XRD results) of the four kinds of samples after corrosion at 345 and 545 °C for 10 h are the same as our previous studies^[26-28]. A lot of Na₂MgCl₄ and NaMgCl₃ are detected, which are two kinds of phases of the “eutectic composition”. A little MgCl₂·6H₂O, MgO and NaCl are also detected. Except the MgO, other metal oxides cannot be found.

In a word, after corrosion at 345 °C for 80 h, MgO crust forms on the surface of the four kinds of specimens. The specimens’ surface is all incomplete. And there is little change in the content of the Fe, Cr, Ni on the cross section of the three kinds of analog stainless steels. After corrosion at 545 °C, the intergranular corrosion occurs seriously on the

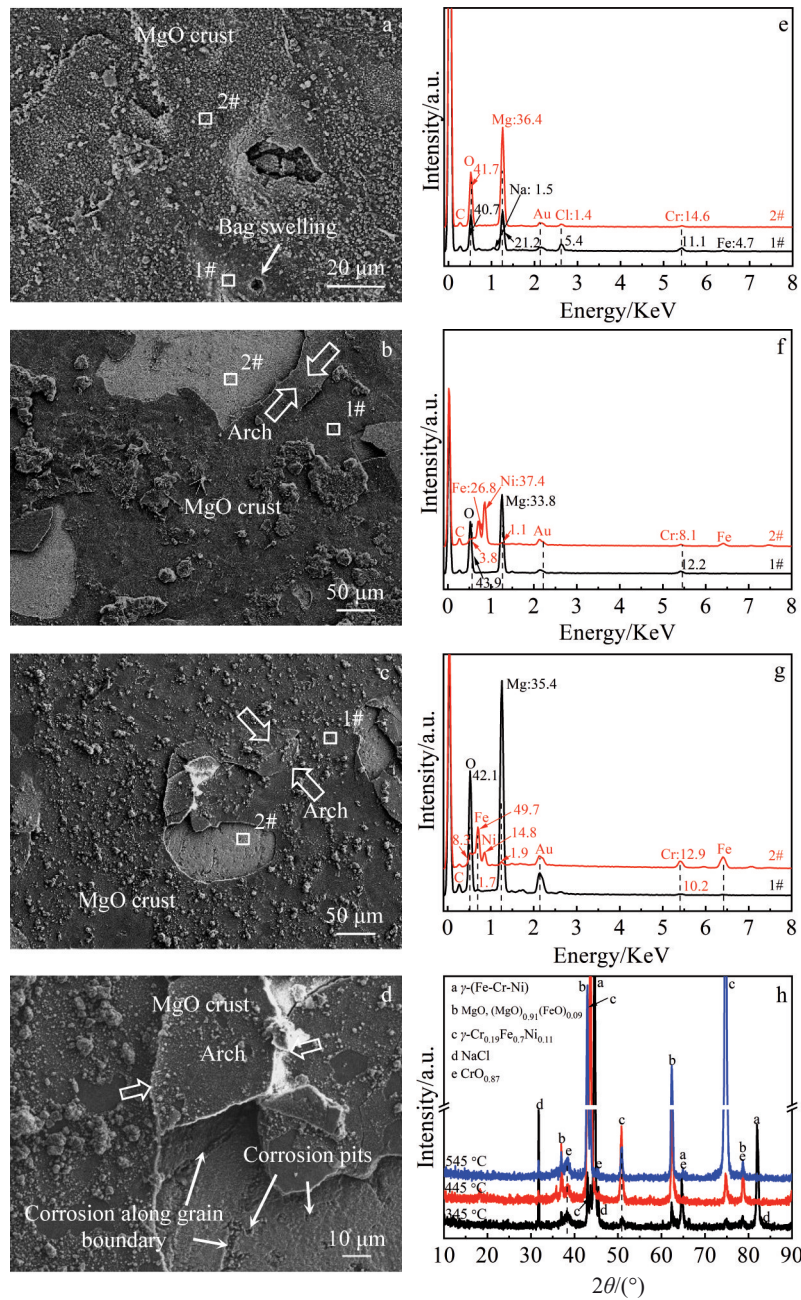
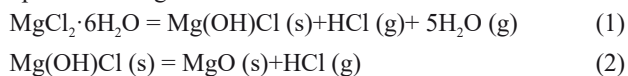


Fig.4 SEM images (a~d), EDS spectra (e~g) and XRD patterns (h) of 304 specimen surface after corrosion at different temperatures for 10 h: (a, e) 345 °C, (b, f) 445 °C, and (c, d, g) 545 °C (numbers in Fig.4e~4g indicate relative content of the element in at%)

carbon steel (T8) surface. For the three kinds of analog stainless steels, MgO crust also forms on their surface. The content of Cr on the specimen surface is lower than that in the matrix. The content of Ni near specimen surface slightly increases or does not significantly change.

2.2 Analysis of corrosion in solid NaCl-MgCl₂ at 345 °C

There is a lot of MgCl₂·6H₂O in the residual salt after corrosion at 345 °C. The MgCl₂·6H₂O forms because the MgCl₂ absorbs moisture during heating process. Then the MgCl₂·6H₂O decomposes into MgO (s) and HCl (g) when the temperature is higher than 175 °C^[11].



As shown in Fig. 8a, before the specimen is put in the molten salt (545 °C), the MgO particle has been excited in the molten salt. When the specimen with low temperature (room temperature) is put in the molten salt, a chilling salt crust forms on the specimen surface. These MgO particles act as heterogeneous nucleated particles, many small solid salt-crystals form around the specimen and adhere to the solid salt crust surface, as shown in Fig.8b.

As the molten salt temperature decreases near the specimen surface, more and more small crystals adhere to the specimen surface. Because the specimen is very smaller than the molten salt in volume, the solid salt crust will melt into the molten salt later. But the MgO particles which have high melting

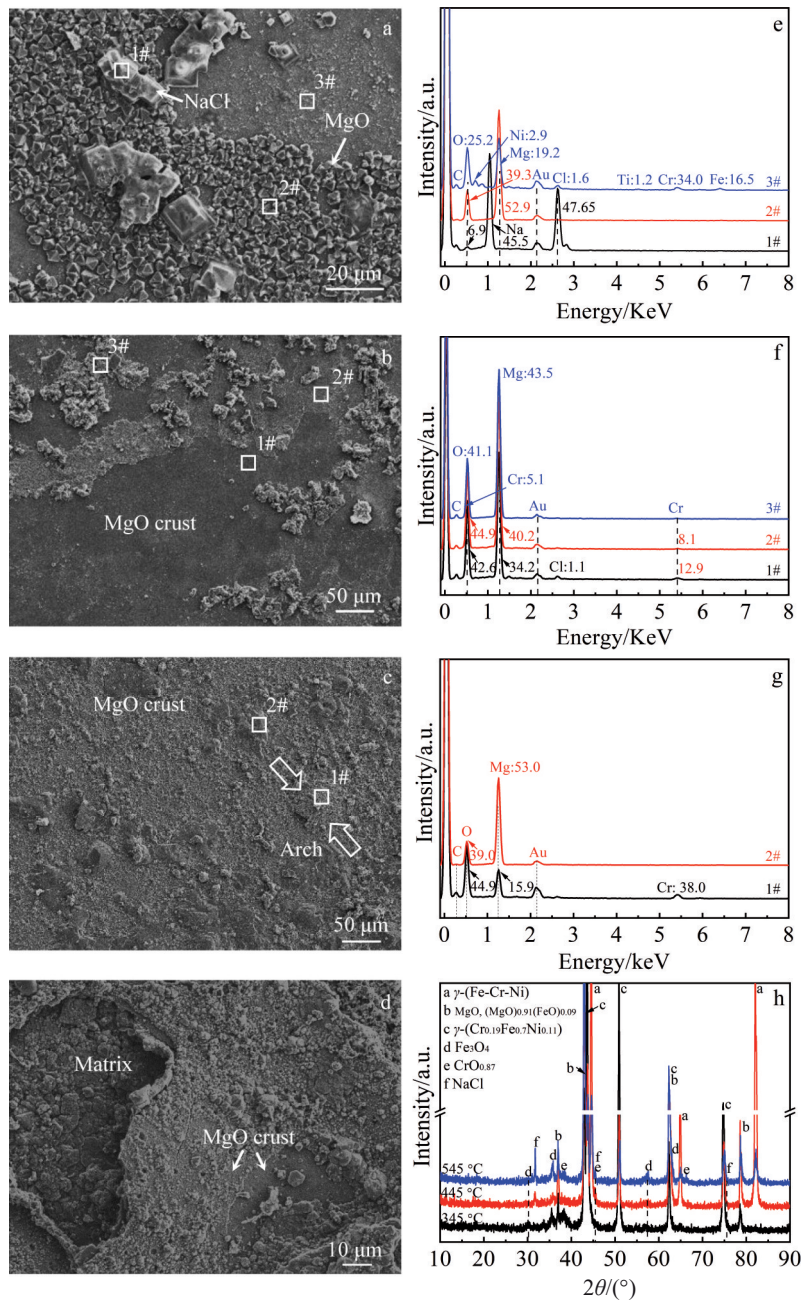


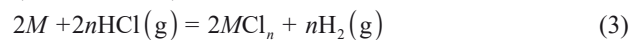
Fig.5 SEM images (a~d), EDS spectra (e~g) and XRD patterns (h) of 321 specimen surface after corrosion at different temperature for 10 h: (a, e) 345 °C, (b, f) 445 °C, and (c, d, g) 545 °C (note that numbers in Fig.5e~5g indicate relative content of the element in at%)

point are gradually deposited on the specimen surface, as shown in Fig.8c.

For the corrosion experiment in the solid mixed salt at 345 °C, after the crucible with molten salt and sample are moved to a muffle furnace of 345 °C, the molten salt solidifies from around of the crucible to the center. Then the specimen with the MgO crust is corroded in the solid salt at 345 °C, as shown in Fig.8d. Because the molten salt shrinks in volume, there are many cracks and holes in the solid salt. The longitudinal section of the bloke salt with the specimen and crucible is shown in Fig.9.

As the reactions of Eq.(1) and Eq.(2) go on, the product HCl (g) will reach the specimen's surface along cracks and

holes in the block salt, and then reacts with the alloy elements M ($M = \text{Fe}, \text{Cr}, \text{Ni}$). The reactions are follows^[18]:



The standard Gibbs free energy changes of Eq. (3) for different alloy elements at 345 °C are shown in Table 3.

In addition, the product HCl (g) in Eq.(1) and Eq.(2) reacts with O_2 (g) in air, as shown in reaction (4).



The Cl_2 will also arrive at the specimen surface along the cracks and holes in the block salt. Then the chlorination reaction occurs as follows^[31]:



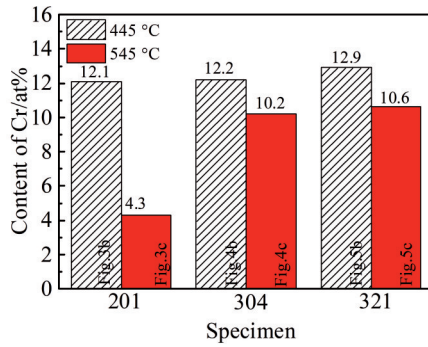


Fig.6 Content of Cr in the analog stainless steels oxide crust at position 1# marked in Fig.3~Fig.5

Table 2 Change and content of alloy elements in the exposed matrix of specimen 304 after corrosion in the molten salt

State of specimen	Element content and change/at%		Position
	Cr	Ni	
As-received	19.2	9.1	-
Corroded at 445 °C	8.1 ↓	37.4 ↑	Position 2# in Fig.4b
Corroded at 545 °C	12.9 ↓	14.8 ↑	Position 2# in Fig.4c

where M is alloy elements of Fe, Cr or Ni. The changes of standard Gibbs free energy of the chlorination reaction (5) at different temperatures are shown in Fig.10.

It is found from Fig.10 that the alloy elements in the four kinds of specimens can react with Cl_2 at the experiment temperature. Consequently, after corrosion for a long time (80 h), the sample surface is incomplete. That is shown in Fig. 7a, 7c, 7e and 7g.

However, the T4 temperature (a temperature, at which chloride vapor pressure is higher than 101.325×10^{-4} kPa^[34]) of the chloride of Fe and Cr is close to the corrosion temperature. The chlorides of Fe and Cr (or hydrous chloride, $\text{MCl}_n \cdot x\text{H}_2\text{O}$), which are generated in Eq.(3) and Eq.(5), volatilize easily and escape from the corrosion system^[26,31]. Or these chlorides will be oxidized when the oxygen partial pressure is high, and then an unprotected oxide film is formed on the specimen surface. Consequently, the chloride of Fe, Cr and Ni cannot be found obviously in the XRD results. In addition, the chloride of Eq.(3) and Eq.(5) is relatively little because of the low content of HCl (g) and Cl_2 (g). Consequently, after corrosion in the solid salt at 345 °C for 80 h, the content change of the element Fe, Cr and Ni is not obvious near surface of the four kinds of specimen matrix, as shown in Fig.7a, 7c, 7e and 7g.

It is also found from Table 3 and Fig. 10 that the standard Gibbs free energy change of the chlorination reaction of Cr is more negative than that of other elements, and the alloy element Cr will react with HCl (g) and Cl_2 (g) preferentially. After the evaporation of reaction products (CrCl_3), the surface of the three kinds of analog stainless steel becomes loose. The

adherence force between the MgO crust and the loose specimen matrix decreases. Consequently, the MgO crust on the stainless-steel surface is loose. The HCl (g) and Cl_2 (g) contact with specimen surface and react with sample matrix continuously. Therefore, the mass of three kinds of stainless steels decreases continuously, as shown in Fig.1.

For the carbon steel specimen, as shown in Fig.7a, the MgO crust inlays the specimen surface by the mechanical occlusion actions, which protects the carbon steel from corrosion by HCl (g) and Cl_2 (g). As a result, the mass of the carbon steel increases after corrosion for 10 h. And the specimen mass gain increases during the corrosion process. The corrosion process of the T8 sample is inhibited under the protected MgO crust.

2.3 Analysis of corrosion in molten NaCl-MgCl₂

In the molten salt, as shown in Fig.8a~8c, the chilling salt crust also forms and remelts again on the specimen surface at the initial stage after the specimen is put in the molten salt. Then a lot of MgO particles are deposited on the specimen surface. However, as ion solution and electrolyte, the molten chloride salt penetrates the MgO layer and reacts with the sample matrix in the form of electrochemical reaction^[24,26].

For the carbon steel, the grain boundary is dissolved preferentially for high energy, which is shown in Fig.2d. The loosed electron is captured by the dissolved oxygen atom (O) in the molten salt. As a cathodic reaction, the oxygen ion (O^{2-}) and MgO (s) form. Those reactions are shown as follows^[26,31]:



where M is Fe, $n=2$ or 3. After corrosion for a long time, the intergranular corrosion occurs, as shown in Fig. 7b. For the conservation of electrons, the chloride of iron (Fe) forms when the chloridion (Cl^-) reacts with the metal ions (such as Fe^{2+} or Fe^{3+}), the reaction is as follows^[11]:



The oxygen ions (O^{2-}) in Eq.(7) not only reacts with the magnesium ions (Mg^{2+}) and produces MgO, but also reacts with the dissolved metal ions in Eq.(6) and produces a metal oxide. A dense mixed oxide layer of $(\text{MgO})_{0.91}(\text{FeO})_{0.09}$ is formed, as shown in Fig.3h, Fig.4h and Fig.5h.

As shown in Fig.2c, because a large area of MgO layer has peeled off, the oxide layer cannot protect the carbon steel sample from corrosion in the molten salt. After grain boundary is corroded thoroughly, a grain on the specimen surface will peel off too, which leads to more mass loss.

For the three kinds of Fe-Cr-Ni alloys, after corrosion in the molten NaCl-MgCl₂, it is found from the change of the alloy element content on the sample surface (Fig.3b~5b and Fig.3c~5c) and the cross section (Fig.7b, 7d, 7f, 7h) that the element Cr is depleted near sample surface. The chromium (Cr) depletion phenomena in the Fe-based and Ni-based specimens is also found after corrosion in other kinds of molten chloride salt^[22,35]. The polarization curves of the alloy specimens in the molten chloride show that for the nickel (Ni)-based alloy, the corrosion potential of the Haynes 224 with high content of the

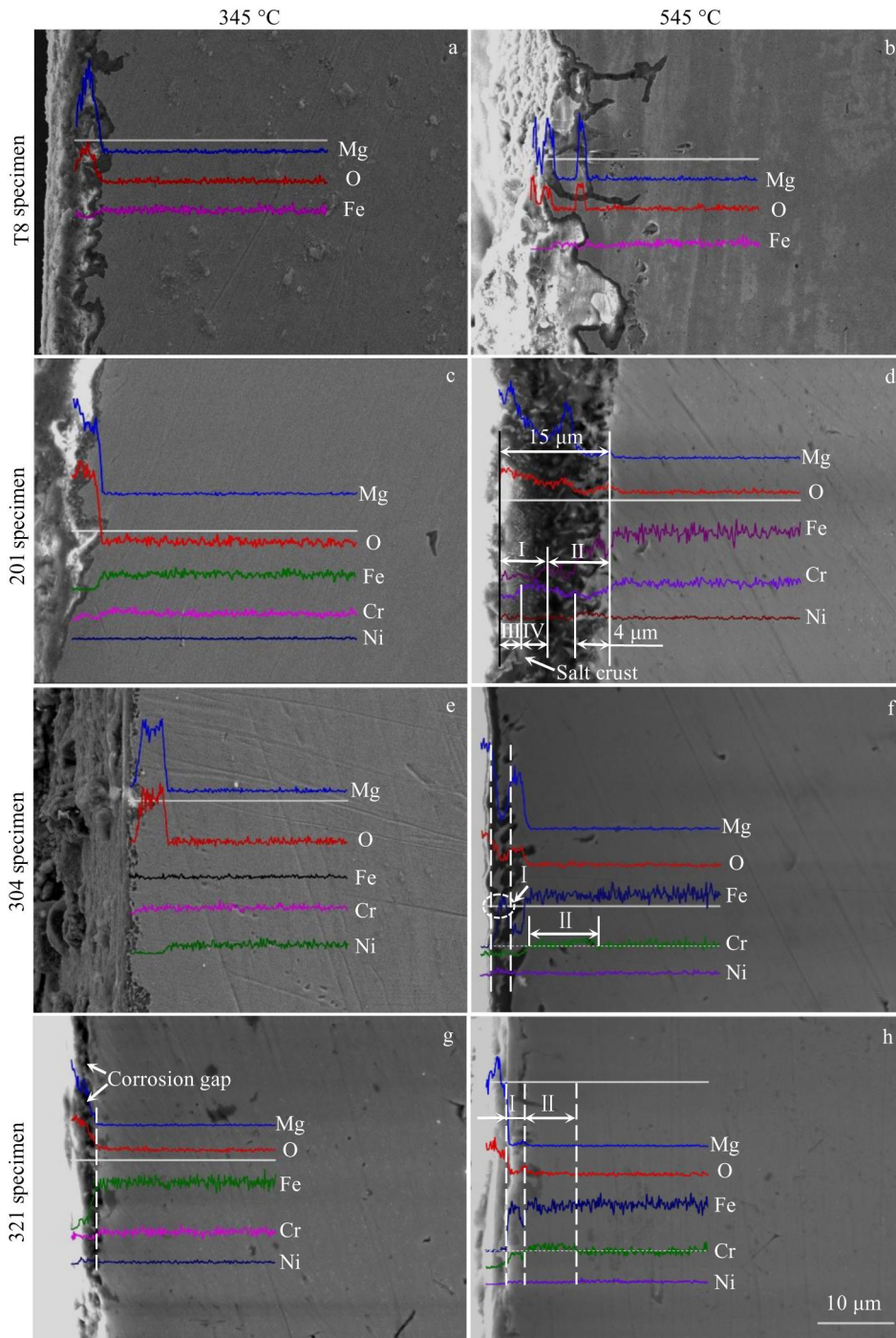


Fig.7 Cross section SEM images and EDS results of four kinds of specimens after corrosion at different temperatures for 80 h

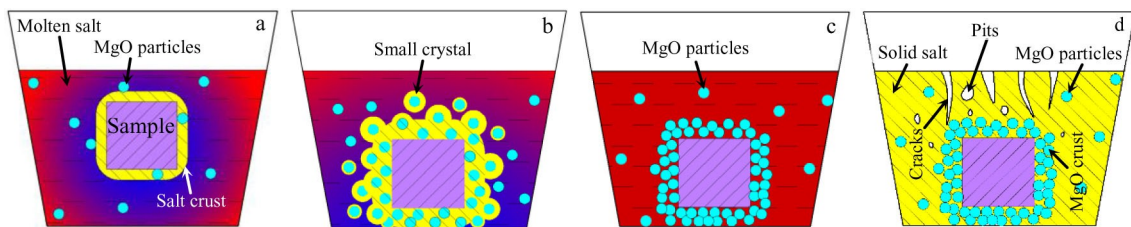


Fig.8 Schematic diagrams of the salt crust change: (a) salt crust formation, (b) crystallization, (c) remelting, and (d) after solidification

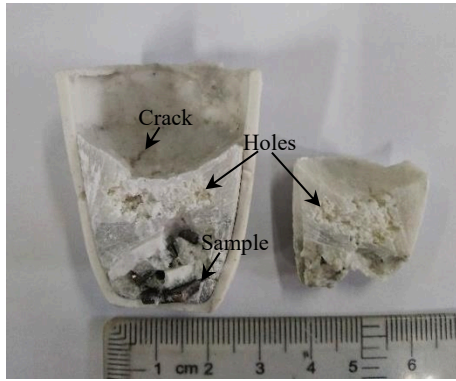


Fig.9 Longitudinal section of solid salt with specimens and crucible

Table 3 Standard Gibbs free energy changes of alloy elements (M) reacting with 1 mol HCl at 345 °C (kJ/mol)

FeCl ₂	FeCl ₃	CrCl ₂	CrCl ₃	NiCl ₂
-32.8	8.2	-60.0	-44.2	-7.3

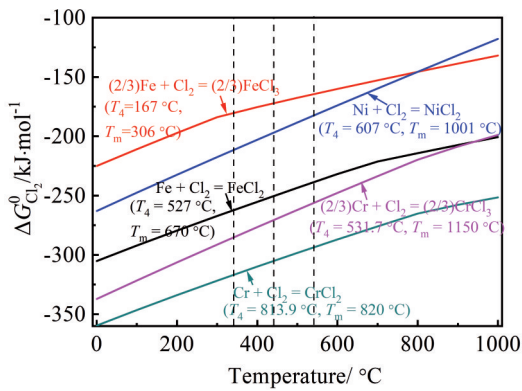


Fig.10 Standard Gibbs free energy changes of chlorination reaction in Eq.(5) at different temperatures^[32,33]

chromium (20.5wt%) is lower than that of the Inconel 702 with low content of Cr (14wt%~17wt%)^[22]. For the Fe-based alloy, the corrosion potential of the specimen SS310 with high content of Cr (25.0wt%) is also lower than that of the specimen SS347 (Cr 17.67wt%). Consequently, the corrosion potential values of the analog stainless steels decrease with the addition of the alloy element Cr. The alloy elements Cr as an anode will be dissolved in the molten salt preferential to Fe and Ni. Then the reactions of the chlorination, oxidation, and

reduction reactions occur like Fe discussed above. As a result, the content of Cr decreases near sample surface obviously, as shown in zone II in Fig. 7d, zone I in Fig. 7f and Fig. 7h. The content of the elements nickel (Ni) relatively increases for the depletion of chromium (Cr) near specimen surface.

The dissolved Cr³⁺ will also be oxidized like Mg²⁺ according to Eq.(8). Then an oxide of chromium (CrO_{0.87}) or a mixture of MgO and CrO_{0.87} is formed. However, the oxide of the chromium easily dissolves in molten chloride in the form of alkaline dissolution^[33]. As shown in Fig.7d, in zone I, after the CrO_{0.87} dissolves from the MgO crust, the content of Cr decreases from the crust bottom to surface. The higher the exposure temperature, the greater the dissolution of the CrO_{0.87} in the molten salt. Consequently, as shown in Fig. 6, the contents of Cr in the smooth oxide crust on the three kinds of stainless-steel surface after exposure at 545 °C are all lower than that at 445 °C.

Although the compound of the chromic (Cr) cannot be detected by XRD in the corrosion residual salt, as reported in Ref. [35], the content of Cr is relatively high in the residual salt after the specimen with chromium (Cr) is corroded in molten chloride.

As a decomposition product of reactions in Eq. (1), Eq.(2) and Eq. (4), the Cl₂ dissolves into the molten salt and reacts with the metal atoms by Eq. (5). Consequently, the corrosion mechanisms of this iron-based alloys in the molten chloride are the chemical-electrochemical combination reactions.

The porous microstructure forms on the stainless-steel sample surface after the alloy element chromium (Cr) runs off, which is shown in Fig. 3d, 4d, and 5d. After exposure for a long time (80 h), it is found from the cross section of specimen 201 (Fig. 7d) that the microstructure near specimen surface is very loose, which reduces the bonding strength of the magnesium oxide (MgO) crust and the matrix too.

The oxide crust on three kinds of simulated stainless-steel surface is mostly MgO, and a little mixed oxide of Fe and Cr ((MgO)_{0.91}(FeO)_{0.09} and CrO_{0.87}). Consequently, the alloy elements Fe and Cr cannot be oxidized completely in the molten chloride salt because of low oxygen partial pressure. The oxide crust is deposited on the specimen surface, rather than formed by consumptive metal atoms on the specimen surface. Consequently, the oxide crust peels off mostly under thermal stress, rather than PBR (Pilling-Bedworth ratio).

As shown in Fig. 11a and 11b, because the thermal expansion coefficient of the Fe-Cr-Ni austenitic stainless steel

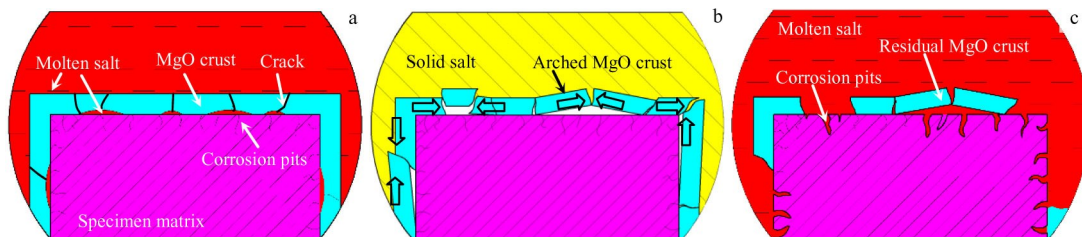


Fig.11 Schematic diagrams of cracking and peeling off of MgO crust in the cooling and remelting process of molten salt: (a) in molten salt, (b) after freezing, and (c) remelting

($17 \times 10^{-6} \text{ K}^{-1}$) is larger than that of the magnesium oxide (MgO , $13.22 \times 10^{-6} \text{ K}^{-1}$)^[36], the MgO crust formed on the specimen surface at 445 and 545 °C endures compressive stress after the specimen is cooled to room temperature. When the compressive stress is high enough, the MgO layer will arch and peel off, as shown in Fig. 2~5 (marked by hollow arrows).

When the specimens in the mixture salt are heated to melt again, the molten salt penetrates the MgO /specimen interface easily, and then series of chemical-electrochemical reactions of Eq. (3), Eq. (5), Eq. (6) and Eq. (9) take place. The sample surface becomes loose, which exacerbates corrosion and the peeling off of the MgO crust. The schematic diagram is shown in Fig. 11c.

3 Conclusions

1) In solid NaCl-MgCl_2 mixture (345 °C), MgO crust forms on the carbon steel specimen surface, which adheres to the surface tightly and protects the specimen from corrosion by HCl and Cl_2 .

2) MgO crust also forms on the Fe-Cr-Ni alloy surface after exposure in the NaCl-MgCl_2 at 345 °C. However, because the HCl and Cl_2 penetrate the sample/ MgO interface along cracks or holes in the solid salt and MgO crust, surface microstructures become loose and corroded severely. The adherence force between the MgO crust and the specimen matrix also decreases for the loose microstructure, which exacerbates corrosion after the MgO crust peels off.

3) In molten NaCl-MgCl_2 , MgO crust on the carbon steel and Fe-Cr-Ni alloy surface cracks and peels off for the thermal stress, which cannot protect sample from corrosion: the corrosion rate of the carbon steel is very high because the grain boundary is corroded preferentially as an anode. The alloy element Cr in the Fe-Cr-Ni samples is dissolved preferentially in the form of alkaline dissolution and volatilized in the form of CrCl_3 , which leads to high corrosion rate.

References

- Rodata S, Abanadesa S, Boujjatbc H et al. *Renew Sustain Energy Rev*[J], 2020, 132: 110 061
- Li Z, Lu Y, Huang R et al. *Applied Energy*[J], 2021, 283: 116 277
- Myers Jr P D, Goswami D Y. *Appl Therm Eng*[J], 2016, 109: 889
- Mehos M, Turchi C, Vidal J et al. *Concentrating Solar Power Gen3 Demonstration Roadmap*[R]. US: NREL, 2017
- Wang J W, Bao Z L, Ye H H et al. *Rare Metal Materials and Engineering*[J], 2020, 49(2): 412
- Wei X L, Song M, Wang W L et al. *Appl Energy*[J], 2015, 156: 306
- Kenisarin M M. *Renew Sustain Energy Rev*[J], 2010, 14: 955
- Li X J, Li N, Liu W H et al. *Sol Energy Mater Sol Cells*[J], 2020, 210: 110 504
- Sun H, Wang J Q, Tang Z F et al. *Corros Sci*[J], 2020, 164: 108 350
- Rapp R A. *Mater Sci Eng*[J], 1987, 87: 319
- Wang J W, Zhou H X, Zhang C Z et al. *Sol Energy Mater Sol Cells*[J], 2018, 179: 194
- Ruiz-Cabañasa F J, Prietoa C, Madinab V et al. *Sol Energy Mater Sol Cells*[J], 2017, 163: 134
- Guo L L, Liu Q, Yin H Q et al. *Corros Sci*[J], 2020, 166: 108 473
- Nishikata A, Shimatani Y, Haruyama S. *J Japan Inst Metals*[J], 1984, 48: 705
- Ishitsuka T, Nose K. *Corros Sci*[J], 2002, 44: 247
- Li X J, Liu W H, Tang Z F et al. *J Mol Liq*[J], 2020, 314: 113 596
- Chen H Z, Li B R, Wen B et al. *Corros Sci*[J], 2020, 173: 108 798
- Sun H, Zhang P, Wang J Q. *Corros Sci*[J], 2018, 143: 187
- Gomez-Vidal J C, Fernandez A G, Tirawat R et al. *Sol Energy Mater Sol Cells*[J], 2017, 166: 222
- Liu B, Wei X L, Wang W L et al. *Sol Energy Mater Sol Cells*[J], 2017, 170: 77
- Wallace A J. *Molten Chloride Salts for Heat Transfer in Nuclear Systems*[D]. Ann Arbor: The University of Wisconsin-Madison, 2011
- Gomez-Vidal J C, Fernandez A G, Tirawat R et al. *Sol Energy Mater Sol Cells*[J], 2017, 166: 234
- Ushak S, Marin P, Galazutdinova Y et al. *Appl Therm Eng*[J], 2016, 107: 410
- Romo L, Gonzalez-Rodriguez J G, Porcayo-Calderon J et al. *Intermetallics*[J], 2015, 67: 156
- Hofmeister M, Klein L, Miran H et al. *Corros Sci*[J], 2015, 90: 46
- Wang J W, Zhang C Z, Li Z H et al. *Sol Energy Mater Sol Cells*[J], 2017, 164: 146
- Wang J W, Zhou H X, Zhong R J et al. *Rare Metal Materials and Engineering*[J], 2017, 46(4): 935
- Zhou H X, Wang J W. *Trans Mater Heat Treatment*[J], 2017, 38: 164 (in Chinese)
- Xu T R, Li X J, Guo L L et al. *Sol Energy*[J], 2020, 209: 568
- Liu Q, Wang Z R, Liu W H et al. *Corros Sci*[J], 2021, 180: 109 183
- Ding W J, Shi H, Jianu A et al. *Sol Energy Mater Sol Cells*[J], 2019, 193: 298
- Ishitsuka T, Nose K. *Mater Corros*[J], 2000, 51: 177
- Wang J W, Bao Z L, Xiang R Q et al. *Mater Chem Phys*[J], 2020, 243: 122 392
- Bender R, Schütze M. *Mater Corros*[J], 2003, 54: 567
- Gomez-Vidal J C, Tirawat R. *Sol Energy Mater Sol Cells*[J], 2016, 157: 234
- Hirata Y. *Ceram Int*[J], 2015, 41: 2706

腐蚀产物MgO对Fe基合金在固态和熔融NaCl-MgCl₂中高温耐蚀性能的影响

常丽梅¹, 张世洲¹, 文 茜¹, 席吉辉¹, 吴 波², 王军伟^{2,3}

(1. 青海大学 机械工程学院, 青海 西宁 810016)

(2. 集美大学 厦门市海洋腐蚀与智能防护材料重点实验室, 福建 厦门 361021)

(3. 青海大学 青海省高性能轻金属合金及深加工工程技术研究中心, 青海 西宁 810016)

摘 要: 熔融氯化盐是下一代聚光式太阳能热发电站(第3代CSP)候选传热和储热介质, 含MgCl₂的熔融氯化盐对金属传热管道和储热容器腐蚀后在其表面形成MgO, MgO对管道耐腐蚀性能影响尚不清楚。通过对比碳钢和3种Fe-Cr-Ni合金在固态(345 ℃)和熔融NaCl-MgCl₂(445和545 ℃)中的腐蚀行为, 分析了MgO对4种试样在不同温度下的腐蚀行为机理。结果表明, 在固态NaCl-MgCl₂中, 碳钢表面MgO壳致密且连续, 可以保护试样免受腐蚀。在熔融NaCl-MgCl₂中, 4种试样表面也生成了致密的MgO壳, 但它因热应力作用而开裂和剥落, 熔融盐沿着氧化膜裂纹渗入MgO/基体界面, 发生化学-电化学联合腐蚀反应, 不能保护试样免受该熔盐腐蚀。

关键词: Fe-Cr-Ni合金; 碳钢; 熔融氯化盐; 腐蚀; MgO

作者简介: 常丽梅, 女, 1995年生, 硕士生, 青海大学机械工程学院, 青海 西宁 810016, 电话: 0971-5310440, E-mail: 3064496651@qq.com